Journal of Photochemistry and Photobiology A: Chemistry 223 (2011) 132–139

Contents lists available at SciVerse ScienceDirect

Journal of Photochemistry and Photobiology A: Chemistry

journal homepage: www.elsevier.com/locate/jphotochem

IR laser deposition: Co_2Sm_5 nanocrystals in amorphous Sm–Co phase and amorphous Sm–Co nanobodies in carbonaceous phase

J. Pola[a,*], D. Pokorná[a], M. Maryško[b], Z. Bastl[c], J. Šubrt[d], S. Bakardjieva[d], P. Bezdička[d], M.A. Gondal[e], H.M. Masoudi[e]

[a] Laboratory of Laser Chemistry, Institute of Chemical Process Fundamentals, ASCR, 16502 Prague, Czech Republic
[b] Institute of Physics, ASCR, 18223 Prague 8, Czech Republic
[c] J. Heyrovský Institute of Physical Chemistry, ASCR, 18223 Prague, Czech Republic
[d] Institute of Inorganic Chemistry, ASCR, 25068 Řež, Czech Republic
[e] Electrical Engineering Physics Departments, King Fahd University of Petroleum & Minerals, 31261 Dhahran, Saudi Arabia

ARTICLE INFO

Article history:
Received 12 May 2011
Received in revised form 27 July 2011
Accepted 13 August 2011
Available online 22 August 2011

Keywords:
IR laser
$SmCo_5$
Sm–Co phases
Gas-phase deposition
Magnetic properties
Nanoalloys

ABSTRACT

Pulsed IR laser irradiation of $SmCo_5$ alloy in vacuum and in adjacent dielectric breakdown (DB) of benzene has been examined as a tool for modifying phase and composition of this alloy and for suitability to serve as a laser deposition technique of Sm–Co nanoparticles and Sm–Co/C films. The composition of solid deposits was determined by FTIR, X-ray photoelectron and Raman spectroscopy and electron microscopy, and gas-phase chemical changes upon irradiation in gaseous benzene were analyzed by gas chromatography and FTIR and GC/MS spectroscopy. IR laser ablation in vacuum leads to deposition of amorphous $Sm_{1.00}Co_{2.1–2.2}$ films containing uniformly dispersed Co_2Sm_5 nanocrystals and to formation of residual Sm_2Co_{17} target phase, both of which indicating disproportionation of $SmCo_5$ and Sm-enrichment of ablated particles. IR laser ablation in benzene results in formation of ultrafine powders consisting in fully amorphous $Sm_{1.00}Co_{4.2–4.6}$ nanoparticles embedded in amorphous hydrogenated carbonaceous phase and is in keeping with minor structural changes in ablated $SmCo_5$ particles. Both deposited materials are shown to differ in magnetic properties and the carbonaceous shell serves as a protection of Sm–Co nanobodies towards atmospheric oxidation.

1. Introduction

There is continuing interest in developing new nanocomposites and methods for their formation. Nanoparticles and nanostructured films based on Sm/Co alloy belong to the class of magnetic materials extensively studied for their intrinsic properties and promising applications in opto- and microelectronics, magnetic energy storage and medicine. Thin epitaxial, amorphous and nanostructured Sm–Co films have been deposited by magnetron sputtering [1–4], near-IR Nd:YAG laser [5], UV laser [6–9] or visible Nd:YAG laser [10,11] ablation of elemental and alloy targets. The Sm–Co (mostly $SmCo_5$) nanoparticles were obtained by chemical (polyol) route [12–18], ball milling [19,20], surfactant-assisted ball milling [21–23] and a pulsed femtosecond laser ablation of Sm–Co alloy in liquid cyclopentanone [24].

The bulk alloy precursors preferred for deposition of nanoparticles and nanostructured films are $SmCo_5$ and Sm_2Co_{17} which are the most important permanent magnets from among several intermetallic compounds of binary Sm–Co equilibrium phase diagram. However, nanoparticles produced from these bulk alloys upon exposure to high energy sources undergo amorphization and composition deviations due to decomposition to different phases [4] and constituents as observed with, e.g. magnetron sputtering [3,4], laser vaporization [5], ball milling [20,21,23], annealing [20], femtosecond laser ablation [24] and possibly with other deposition methods when some disordered nanoproducts were not detected by XRD technique.

The produced Sm–Co nanoparticles (or nanostructured films) are also prone to oxidation which is detrimental to their magnetic properties. Such oxidation can be avoided in surfactant-assisted ball milling [21–23], by addition of polymer [15] or long chain organic compounds in the course of direct chemical synthesis [12,16–18], or by subsequent inclusion in polymer matrix [24]. Alternative protection of Sm–Co nanoparticles has been achieved in the process of gas condensation in a cluster gun by embedding the nanoparticles in a co-sputtered carbon phase [25]. The coated particles are air-stable, have lower coercivity than bare particles, do not loose their magnetic properties within several days and their aggregates remain magnetically stable for months.

We have recently reported on pulsed IR laser ablative deposition of nanoforms of metals surrounded by carbonaceous phase [26–29]. The used single-pulse technique enables simultaneous laser

* Corresponding author. Tel.: +420 2 20390308; fax: +420 2 20920661.
E-mail address: pola@icpf.cas.cz (J. Pola).

1010-6030/$ – see front matter © 2011 Elsevier B.V. All rights reserved.
doi:10.1016/j.jphotochem.2011.08.010

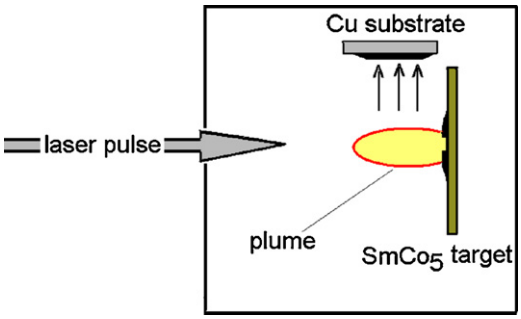

Fig. 1. Scheme of gas-phase deposition.

ablation of metal target in adjacent plume (dielectric breakdown) of decomposing hydrocarbon to achieve laser chemical vapor deposition (LCVD) of metal nanobodies dispersed in amorphous graphitic environment which protects metal nanoparticles towards oxidation.

We were interested to apply this technique for study of IR laser ablation of bulk $SmCo_5$ alloy and to determine phase and composition changes in this alloy in the intense IR laser field as well as to ascertain spectral and magnetic properties of the ablatively deposited products.

2. Experimental

IR-laser irradiation experiments were carried out in a Pyrex reactor (70 mL in volume) in vacuum and at 3 Torr of benzene by using a pulsed TEA CO_2 laser (model 1300 M, Plovdiv University) operating with a frequency of 1 Hz on the P(20) line of the $00^01–10^00$ transition (944.19 cm^{-1}) and a pulse energy of 1.8 J. The radiation was focused with a NaCl lens (f.l. 15 cm) on the $SmCo_5$ disc positioned in the center of the reactor above which were accommodated copper and silica substrates. A simple irradiation scheme is given in Fig. 1. The irradiation of $SmCo_5$ target in vacuum with 300 pulses resulted in ablation of the alloy and deposition of nanosized Sm/Co film, whereas that carried out with 60 pulses at 3 Torr of benzene and repeated 20 times allowed ablation of the alloy in the adjacent dielectric breakdown of benzene and resulted in deposition of Sm/Co/carbon nanocomposite powder.

The reactor was described elsewhere [26] and it was a Pyrex tube fitted at each end with KBr windows and having a port with rubber septum enabling GC and GC/MS analyses of gaseous content, and a PTFE valve connecting to vacuum manifold and pressure transducer.

The progress of benzene decomposition and volatile decomposition products were analyzed directly in the reactor by FTIR spectrometry (an FTIR Nicolet Impact spectrometer, resolution 4 cm^{-1}) using diagnostic absorption band of benzene at 1037 cm^{-1}. Aliquots of the irradiated reactor content were sampled by a gas-tight syringe and analyzed by gas chromatography–mass spectroscopy (a Shimadzu QP 5050 mass spectrometer, 50-m Porabond capillary column, programmed temperature 30–200 °C). The decomposition products were identified through their FTIR spectral diagnostic bands (C_2H_2, 731 cm^{-1}; C_4H_2, 628 cm^{-1}; CH_4, 1305 and 3016 cm^{-1}) and through their mass spectra using the NIST library.

The deposited films were analyzed with the FTIR Nicolet Impact spectrometer, a Nicolet Almega XR Raman spectrometer (resolution 2 cm^{-1}, excitation wavelength 473 nm and power 10 mW) and an ESCA 310 (Scienta) electron spectrometer with a base pressure better than 10^{-9} Torr using Al Kα radiation (1486.6 eV) for electron excitation. The Raman spectral analysis was carried out on different microregions of the deposited layer to verify the homogeneity of the film on Cu substrate and to detect differences in the spectra for the film areas near the target crater. The X-ray C 1s, O 1s and Co $2p_{3/2}$ and Sm $3d_{5/2}$ photoelectron and C KLL Auger electron spectra of the deposit were measured and surface composition of the deposited film was determined by correcting the spectral intensities for subshell photoionization cross-sections.

Further analyses were made by electron microscopy (a Philips XL30 CP scanning electron microscope equipped with an energy-dispersive analyzer EDAX DX-4 of X-ray radiation) and a JEOL JEM 3010 microscope operating at 300 kV and equipped with an EDS detector (INCA/Oxford) and CCD Gatan (Digital Micrograph software). The transmission electron analysis was performed on ground samples that were subsequently dispersed in ethanol followed by application of a drop of a diluted suspension on a Ni grid.

Diffraction patterns were measured with a PANalytical X'Pert PRO diffractometer equipped with a conventional X-ray tube (Co Kα radiation, 40 kV, 30 mA, point focus), an X-ray monocapillary with diameter of 0.1 mm, and a multichannel detector X'Celerator with an anti-scatter shield.

A dual pulsed laser induced breakdown spectroscopy (LIBS) set-up for the analysis of alloy samples (Fig. 2) included two Q-switch pulsed Nd:YAG lasers (Sky lasers) of which the fourth harmonic (266 nm) serves as laser 1 and the fundamental (1064 nm) serves as laser 2. The two lasers are so precisely aligned that the two laser spots fall on the same spot on the sample surface and these aligned laser spots are at the line of sight of the fiber optic detection lens. The adjustable IR and UV lens assembly is used to focus the laser beams on the sample surface. The LIBS signal is collected by the fiber bundle assembly and fed into the seven channels of the LIBS spectrometer (Ocean Optics LIBS 2500 plus). The flash lamps and the Q-switches of both lasers are externally controlled by the LIBS system in the sequence shown in Fig. 2. Laser 1 produces laser induced plasma at the sample surface and after an appropriate time delay after the firing of laser 1, the second laser is fired, which is controlled by the built software in spectrometer of the LIBS system. The second laser is allowed to pass through plume created by the first laser and impinge on the sample surface which enhances the normal LIBS process.

The measurement of the magnetic properties of the prepared Sm/Co films as well as the powder material was carried out using a SQUID magnetometer MPMS-5S (Quantum Design).

Benzene (Lachema, purity better than 99.7 per cent) was subject to three freeze–thaw–evaporation cycles on a vacuum line and admitted to the reactor prior to irradiation. The $SmCo_5$ disk (Aldrich, samarium cobalt alloy 18) was used as delivered.

3. Results and discussion

3.1. IR laser ablation in vacuum

The TEA CO_2 laser irradiation of $SmCo_5$ disc in vacuum by focusing laser pulses to area of 1 mm^2, results in ablation and a visible (yellowish) luminescence (alloy plasma) coming from the $SmCo_5$ surface as a plume confined in a volume of 0.8 cm diameter and 1 cm length. The occurrence of visible plume and the employed irradiation conditions resemble those for IR laser ablative deposition of Co and Ni which were previously confirmed by optical emission spectra to result in transient formation of metal atoms and ions [26].

The EDX-SEM analysis of the deposited film (atomic ratios Sm/Co/Cu = 1.0/2.1–2.2/2.0–2.1) indicates that Sm–Co alloy does not provide full coverage of the substrate and that Co content is much lower than in the initial sample. The deposited film consists of a smooth layer and particles ranging from less than 1 up

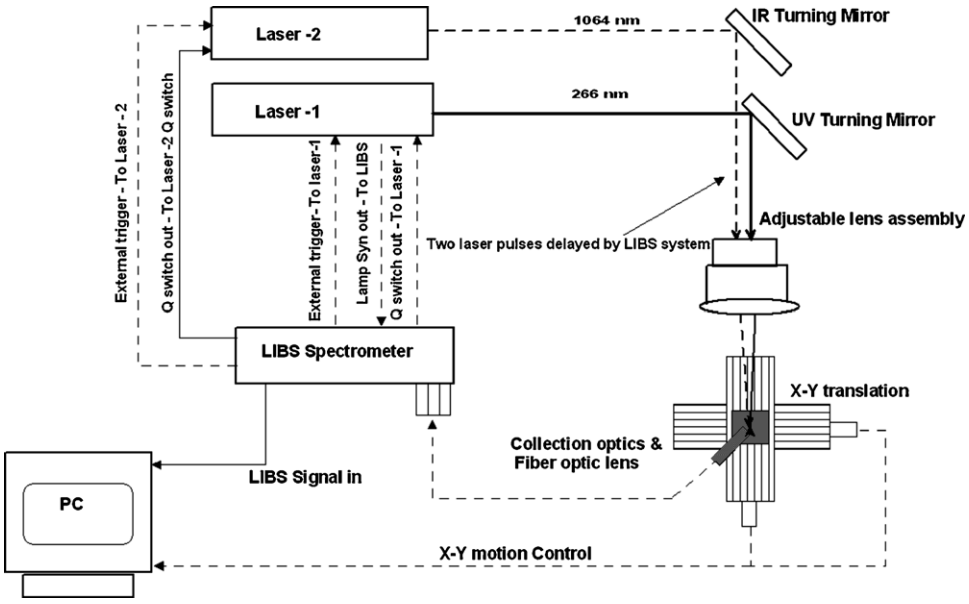

Fig. 2. Schematic diagram of experimental setup of dual pulsed LIBS system for characterization of $SmCo_5$ alloy sample.

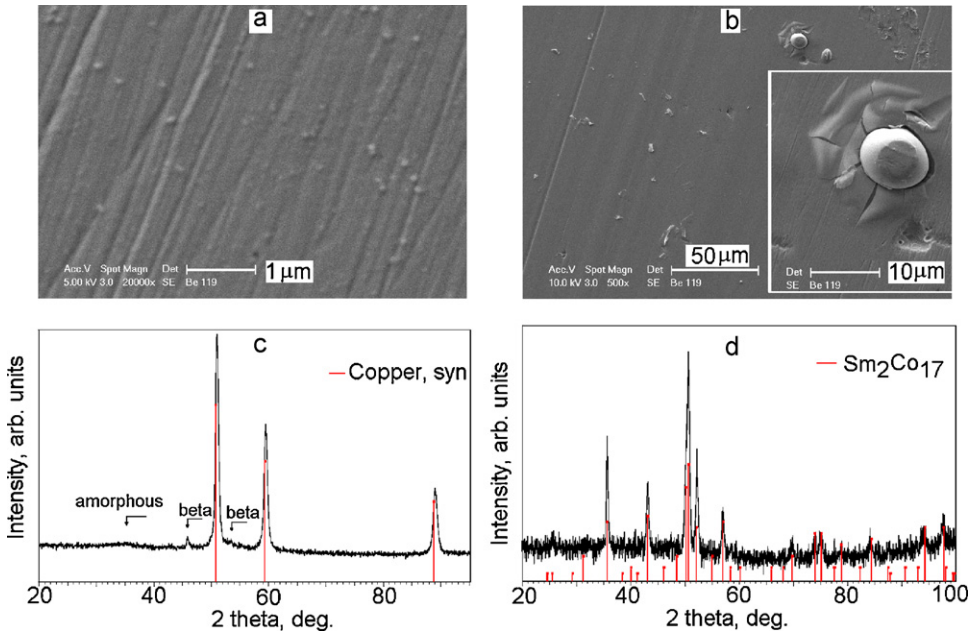

Fig. 3. SEM images of film (and particles) deposited in vacuum from $SmCo_5$ (a and b), X-ray diffraction pattern of amorphous Sm–Co film on Cu substrate (c) and irradiated $SmCo_5$ target (proving formation of Sm_2Co_{17} phase) (d).

to 10 μm (Fig. 3a and b). Some larger deposited particles deform vicinity of the deposition site (inset of Fig. 3b), which indicates that their high kinetic energy is lost upon collision with substrate surface. The X-ray diffraction analysis of the deposited film is in line with amorphous structure (Fig. 3c) and that of the irradiated target (Fig. 3d) shows hexagonal Sm_2Co_{17} phase (PDF 35-1368 [30]).

The polycrystalline phase possesses low amount of Co_2Sm_5 nanocrystals seen on HRTEM images. In Fig. 4a one can see a bulk Co_2Sm_5 specimen and SAED as an inset. Electron diffraction pattern includes a series of continuous rings and confirms the polycrystalline Co_2Sm_5 consisting of many nanocrystals with a random orientation. Process Diffraction software [31] has shown markers indicating positions of diffraction lines belonging to the monoclinic Co_2Sm_5 (PDF ICDD 30-0457). Indication of monoclinic structure through electron diffraction analysis is illustrated in Fig. 4c: the two arrowed reflections are (5 1 0) and ($\bar{1}$ 1 2) which possess a C2/c (space group) structure with monoclinic symmetry and interplanar distance $d_{(5\,1\,0)}$ = 2.88 Å (see Fig. 4d).

The SAED analysis (atomic ratio Co/Sm 2.0–2.2) performed on many selected areas of the film is in good agreement with the EDX-SEM analysis and proves that Co_2Sm_5 nanocrystals are a minor fraction and uniformly distributed in the amorphous phase.

These observed features thus confirm that the irradiated $SmCo_5$ target undergoes disproportionation into (residual) crystalline Sm_2Co_{17} and an (ablated) amorphous ($SmCo_{2.0–2.2}$) phase containing Co_2Sm_5 nanocrystals. This disproportionation results in enrichment of the deposited phase by Sm.

3.2. IR laser ablation in benzene

The TEA CO_2 laser irradiation of $SmCo_5$ target in the presence of gaseous benzene (3 Torr) leads to a visible luminescence,

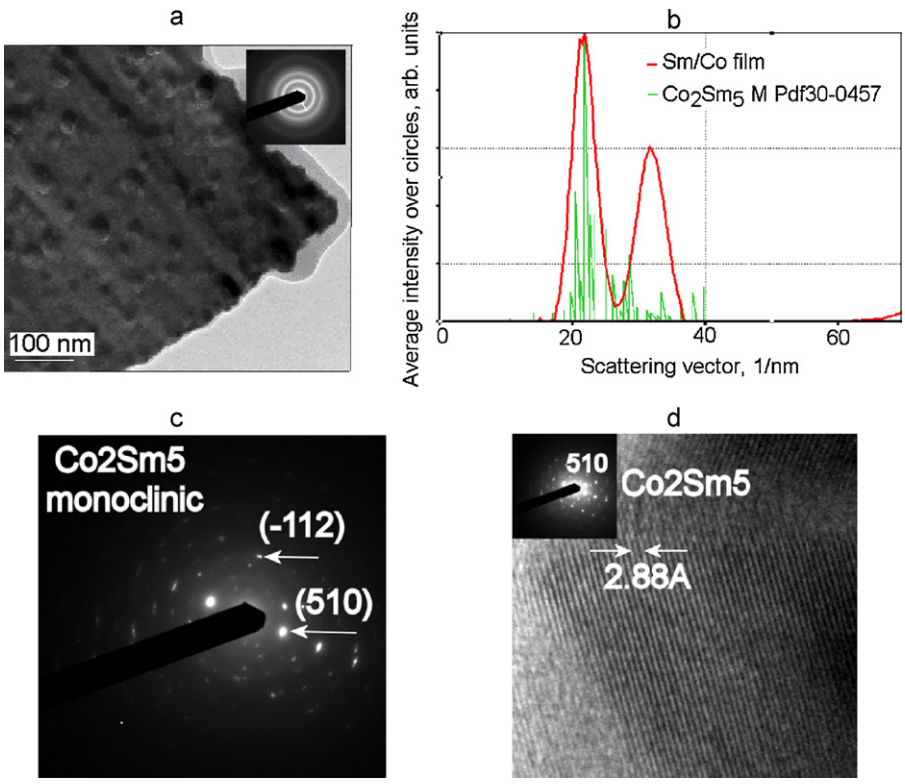

Fig. 4. HRTEM images (a, c, and d) and electron diffraction pattern (b) of the film deposited in vacuum from $SmCo_5$.

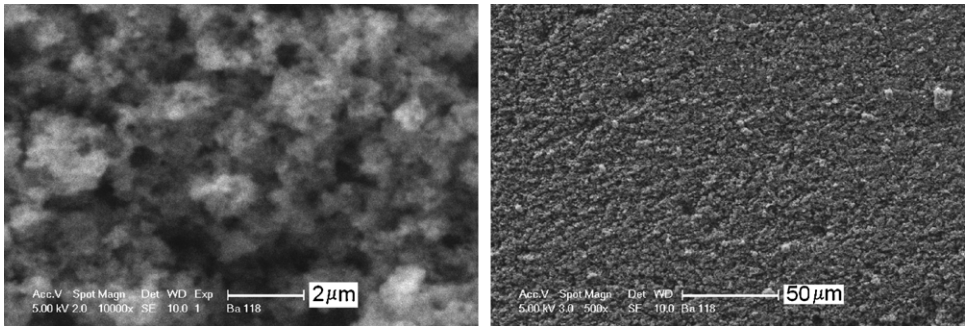

Fig. 5. SEM images of film deposited from $SmCo_5$ at 3 Torr of benzene.

dielectric breakdown in benzene and deposition of a dark Sm–Co/C film. Volatile products of the benzene decomposition are ethyne (~60 mole%), ethene (~20–23 mole%), butadiyne (~10 mole%) and propane, 1-buten-3-yne, C_3H_4, and ethynylbenzene (each 0.1–0.5 mole%) all of which are typical side-products of pyrolytic carbonization of benzene [32]. The repetitive laser pulses lead to accumulation of the mass of products from both $SmCo_5$ ablation and hydrocarbon dielectric breakdown which mostly takes place on the substrates and nearby reactor surface and much less on the surface of the $SmCo_5$ target, where a fraction of the deposit is repeatedly removed by next pulses. The deposit shows low adherence to substrates (Cu and silica) and can be easily moved from the surface of the depositing area as an ultrafine powder.

The SEM-EDX analysis of the deposited film shows fluffy agglomerated structures (Fig. 5) with the prevalence (ca. 90 at.%) of carbon, low amounts of oxygen (less than 2–5 atomic percent of carbon) and low total amounts (less than 3 at.%) of Sm and Co in the ratio Sm/Co = 1/4.2–4.6. The observed ratio is close to that of the initial $SmCo_5$ target, which indicates that ablation is controlled by propelled $SmCo_5$ fragments and that the role of $SmCo_5$ fragmentation and disproportionation is small. We may assume that the irradiation energy is partly consumed for decomposition of benzene and that target surface absorbs less energy, which is favorable for preservation of Sm–Co bonds. The conditions for dielectric breakdown of benzene were similar as in [26] and are in line with concomitant formation of H atoms and neutral and cationic carbon species which give rise to the observed volatile products and carbonization reactions.

The XPS analysis is in good agreement with the SEM-EDX data and shows that the relative atomic content in few superficial layers of the deposited film is Sm: 0.25; Co: 1.00; C: 89.15; O: 9.60. The binding energies for Sm $3d_{5/2}$ and Co $2p_{3/2}$ electrons being respectively 1083.4 eV and 780.1 eV are consistent with both zero-valent and Co(II) and Sm(III) states (e.g.[33,34]). However, these contributions are small and the binding energy of O 1s electrons 531.8 eV being higher than for Sm and Co oxides (~530 eV) allows assignment of the O 1s value to C-OH bonds. Such bonds are typically formed by atmospheric oxidation of C=C bonds which were identified by Raman and Auger spectra in topmost layers of carbonaceous films.

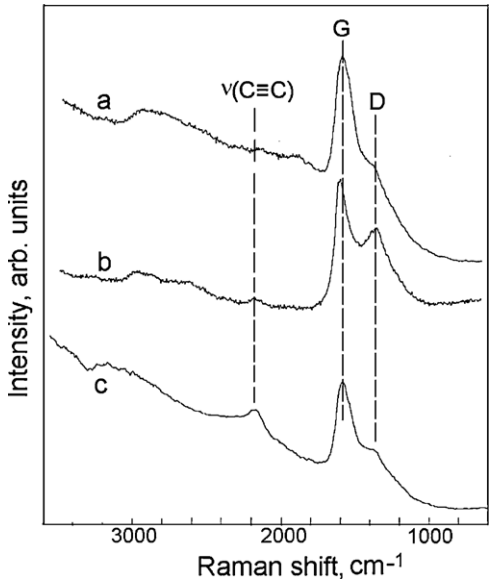

Fig. 6. Raman spectra of film deposited on $SmCo_5$ target far (a) and near (b) the crater, and of film deposited on Cu substrate (c).

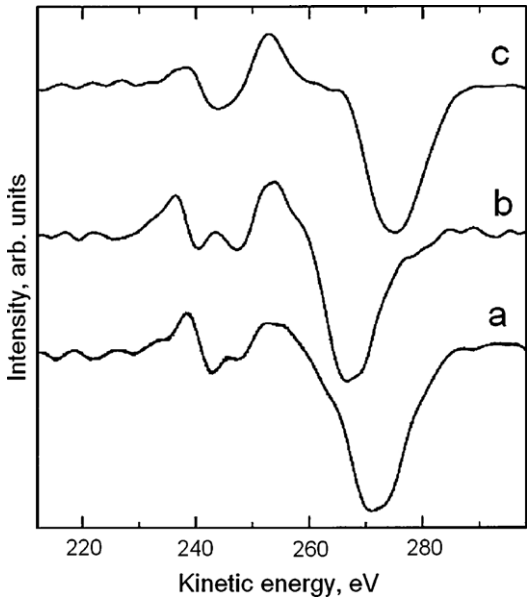

Fig. 7. C KLL X-ray excited derivative Auger spectra of deposited film (a), natural diamond (b) and graphite (c).

The Raman spectra of different regions of the film deposited on Cu substrate and $SmCo_5$ target (Fig. 6) show G and D bands of unsaturated sp^2 carbon, which are respectively centered at 1580–1600 cm^{-1} and 1360 cm^{-1}. The spectra also show a week ν(C≡C) band at 2170–2180 cm^{-1} and a broad band at 2700–3200 cm^{-1} assigned to combination and second harmonic modes and/or C–H stretch vibrations. The positions of D and G bands correspond to graphitic a-C:H films with low sp^3 content [35] having more pronounced graphitic features near the crater of the target (Fig. 6b).

The energy difference between the most positive and most negative excursions in The C KLL derivative Auger spectra were used as a measure of the population of C atoms in sp^3 and sp^2 states (e.g. [36,37]). The comparison of the C KLL spectra of the deposited film with those of reference carbon samples is given in Fig. 7. The separations obtained for diamond and graphite (13.1 eV, and 21.9 eV, respectively) agree well with literature and that for the deposited film (18 eV) corresponds to 70% of sp^2 hybridized C atoms. We therefore infer that topmost layers of such film are easily oxidized in atmosphere.

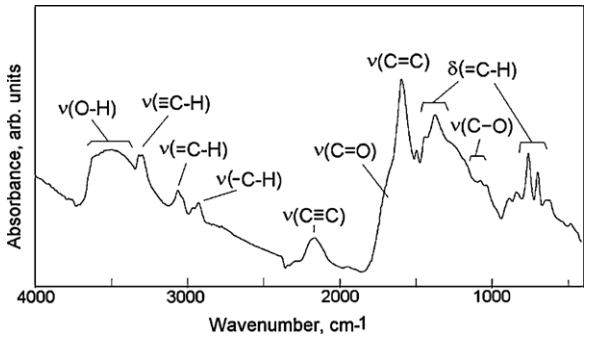

Fig. 8. ATR FTIR spectrum of deposited film.

The ATR FTIR spectra of the deposited film (Fig. 8) confirm that the carbonaceous film contains C–C, C–H, C=C, C–O and C=O bonds [38]. A broad ν(O-H) band is centered at 3500 cm^{-1}, medium ν(≡C–H) band at 3300–3315 cm^{-1}, a ν(=C–H) band at 3060 cm^{-1} and ν(–C–H) bands at 2960 and 2930 cm^{-1} correspond to $C(sp^x)$–H bonds with $x = 1–3$ and are in agreement with in-plane and out of-plane deformation $–C–H_n$ vibrations observed around 1370 and ~650–850 cm^{-1} and with C–C skeletal vibrations at below 700 cm^{-1}. A band at 2165 cm^{-1} relates to C≡C stretch, a strong band at 1590 cm^{-1} corresponds to C=C stretch and weak absorptions above 1600 cm^{-1} and 1100 cm^{-1} relate to C=O and C–O bonds.

The HRTEM analysis of the deposited film (Fig. 9) shows amorphous nanostructured phase containing Sm–Co nanobodies (Fig. 9b) and reveals that the carbonaceous phase resembles (Fig. 9c) curved arrangements of graphene layers [39,40] which are considered as a primary stage of carbon graphitization [41].

The SAED analysis of a number of selected areas of the deposited film is consistent with the Co/Sm ratio = 3.8–4.3 which are values close to those determined by SEM-EDX analyses. These values lend support to small Sm–Co fragmentation in the presence of benzene and show that Sm–Co nanobodies are homogeneously dispersed in the carbonaceous phase.

3.3. Irradiation of $SmCo_5$ with Nd:YAG laser pulses

Typical LIBS spectra recorded for the $SmCo_5$ alloy sample (Fig. 10) represent the Co-line at 345.3 nm and the Sm-line at 429.6 nm (Fig. 10). These spectra were recorded at the surface of the sample (Fig. 10a) and at a depth of few mm (Fig. 10b) by creating a crest in the sample by irradiation of the sample at the same spot. The respective ratios of the areas under the curves (Co–I/Sm–I) are approximately 4.9 and 5.5 and indicate a small enrichment of the irradiated target by Sm. This finding shows a rather high stability of the bulk $SmCo_5$ upon irradiation with 266 and 1064 nm pulses, which contradicts with the dramatic changes induced by the IR laser and with the previously noted partial fragmentation of $SmCo_5$ (formation of Co and Sm (oxidized to Sm_2O_3)) upon vaporization of $SmCo_5$ target with near-IR laser pulses [5].

3.4. Magnetic properties of Sm–Co films and Sm–Co/C powders

The measurements of the magnetic properties of the Sm–Co film deposited from $SmCo_5$ in vacuum, as well as of the ultrafine powder deposited from several experiments at the low pressure of benzene reveals different features. The hysteresis curves at $T = 300$ K and 10 K and temperature dependences of the magnetization M under an applied field $H = 10$ kOe are shown in Figs. 11 and 12.

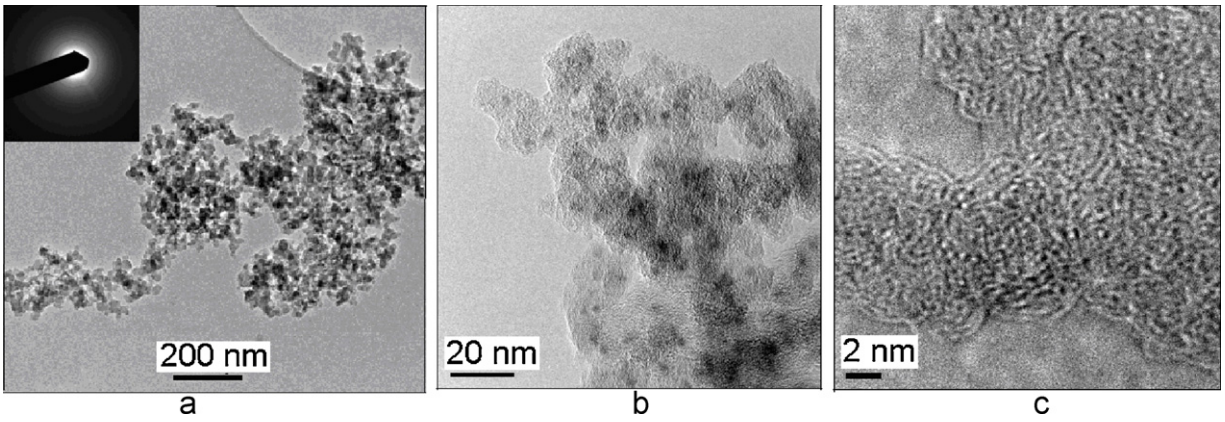

Fig. 9. TEM images of amorphous Sm/Co/C nanocomposite film showing structure of agglomerate (a), incorporation of alloy particles in carbonaceous phase (b) and turbostratic carbon phase (c).

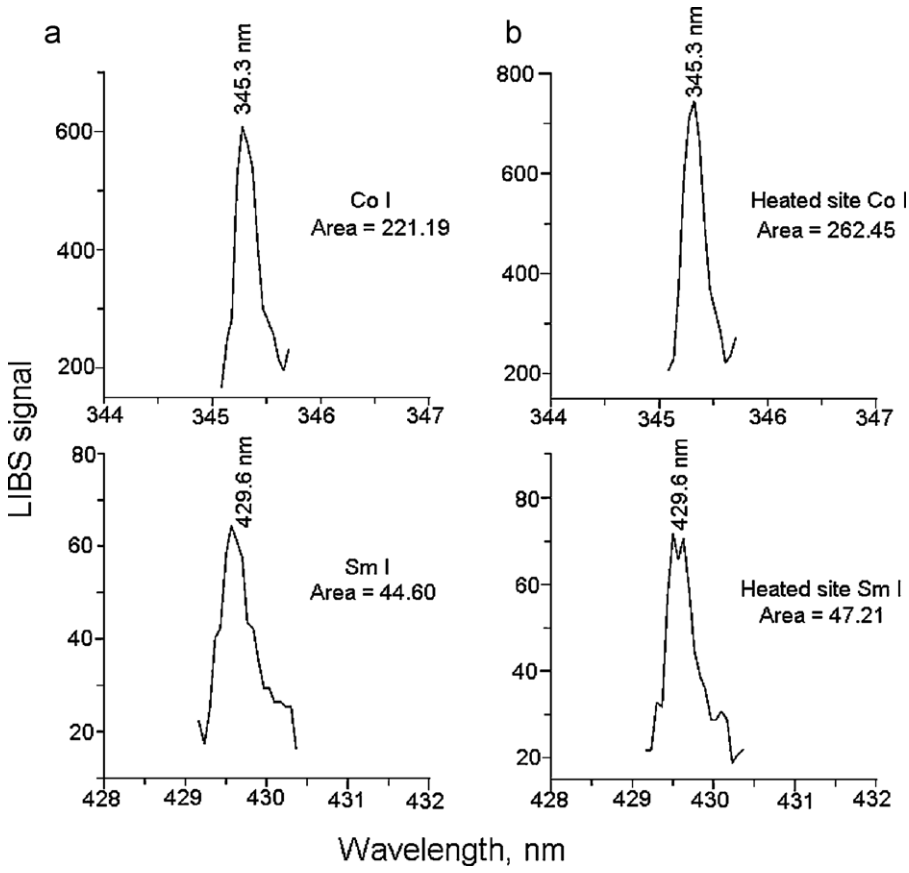

Fig. 10. Dual pulsed LIBS spectra of Sm/Co magnetic alloy characterized on the surface (a) and in the laser-drilled crater (heated site) (b) with atomic lines of Sm–I at 429.6 nm and Co–I at 345.3 nm. The ratio of the areas under the curve Co–I and Sm–I are 4.9 and 5.5, respectively.

The powder material exhibits a non-hysteretic behavior with zero coercivity, which is expected with regard to an isotropic character of the material with no preferential axis. At room temperature the $M(H)$ curve (Fig. 9a) indicates a ferromagnetic (FM) state with a saturation magnetization $M_S \approx 22$ emu/cm^3. The value of M_S was evaluated per unit volume of the $SmCo_5$ phase contained in the powder. (From the EDX-SEM analysis it follows that the weight fraction of $SmCo_5$ is ≈0.5). At $T = 10$ K the magnetization curve can be expressed as a sum of a FM and paramagnetic (PM) contributions. The latter probably corresponds to PM centers formed by Co and Sm atoms. In accord with this interpretation the temperature dependence $M(T)$ (Fig. 11b) represents a superposition of the FM and PM (Curie–Weiss) parts of the total magnetization. We admit, however, that the low saturation magnetization found for the ultrafine Sm–Co/C powder may partly arise from carbon, since low magnetization of carbonaceous powders laser-deposited from the gas phase has been already recognized (e.g. [42,43]).

As a second step we focused our attention on the Sm–Co film with thickness 100 nm deposited on the SiO_2 substrate. In this case the measured values of the magnetic moment were corrected for the diamagnetic contribution of SiO_2 ($\chi = -4.069 \times 10^{-7}$ emu/(g Oe)). The results shown in Fig. 12 were obtained for a parallel configuration with the static magnetic field lying in the plane of the film. For the film, in contrast to the powder material, the hysteresis curves exhibit a finite coercivity, namely H_c (300 K) ≈ 65 Oe, H_c (10 K) ≈ 240 Oe. The absence of

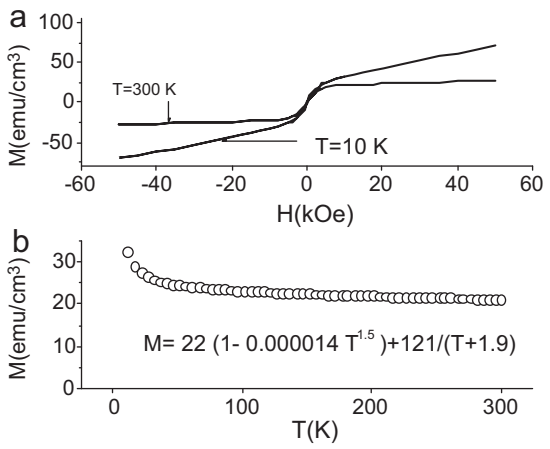

Fig. 11. The magnetic properties of the $Sm_{1.00}Co_{4.2–4.6}$ nanoparticles contained in the carbonaceous powder: (a) hysteresis curves at T = 300 and 10 K and (b) magnetization measured under an applied field 10 kOe.

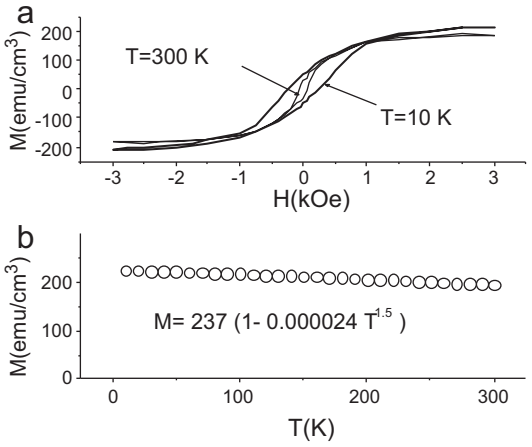

Fig. 12. Magnetic properties of the Sm/Co film; (a) hysteresis curves at T = 300 and 10 K and (b) magnetization vs temperature under an applied field 10 kOe.

a large linear $M(H)$ contribution as well as the temperature dependence which can be approximated by relation $M_0(1 - aT^{3/2})$ suggest the prevailing portion of the FM state (Fig. 12a and b). For a perpendicular configuration M_S remains the same but the values of H_c are larger due to demagnetizing effects. The saturation magnetization M_S (300 K) ≈ 190 emu/cm^3 is comparable with results reported on nanoparticle $SmCo_5$, see e.g. [18]. Let us remark that for nanoparticle materials and thin films the saturation magnetization is always significantly lower when compared with the bulk $SmCo_5$ crystals (M_S = 830 emu/cm^3). On the other hand, the new methods of film preparation can yield the coercivity larger than the bulk value 8.5 kOe [6].

4. Conclusion

IR laser ablation of $SmCo_5$ alloy in vacuum induces deposition of amorphous $Sm_{1.00}Co_{2.1–2.2}$ films containing uniformly dispersed Co_2Sm_5 nanocrystals and leaves the topmost layers of the irradiated target structurally changed through formation of crystalline residual Sm_2Co_{17} phase. The dramatic phase changes indicate disproportionation of $SmCo_5$ and Sm-enrichment of ablated particles.

IR laser irradiation of $SmCo_5$ alloy at low pressure of benzene takes place in adjacent dielectric benzene breakdown and allows deposition of non-adherent layers of amorphous hydrogenated carbonaceous solid which incorporates amorphous $Sm_{1.00}Co_{4.2–4.6}$ nanoparticles. This material indicates very minor structural changes in ablated $SmCo_5$ particles leading to the composition slightly deviating from $SmCo_5$.

UV laser-induced breakdown spectroscopy of $SmCo_5$ alloy induced at 266 and 1064 nm shows that Sm/Co signal ratio little changes upon prolonged irradiation and that the irradiated target becomes slightly enriched by Sm.

Magnetic properties of the Sm–Co film deposited in vacuum and of ultrafine Sm–Co/C powder deposited in benzene show different features: the former has a finite coercivity and saturation magnetization (M_S (300 K) ≈ 190 emu/cm^3), whereas the latter exhibits a non-hysteretic behavior with zero coercivity and saturation magnetization M_S (300 K) ≈ 22 emu/cm^3.

The technique of IR laser ablation of $SmCo_5$ in dielectric breakdown of benzene allows formation of Sm–Co nanoparticles homogeneously distributed in an amorphous graphitic carbon containing C–H bonds and undergoing oxidation in superficial layers. The carbonaceous phase acts as a protecting shell which prohibits oxidation of Sm–Co nanoparticles in atmosphere.

Acknowledgements

The authors thank King Fahd University of Petroleum & Minerals for support of the project #IN090025. Funding by Ministry of Education, Youth and Sports of the Czech Republic (grant no. LC523) and assistance of Dr. Siddiqui is also appreciated.

References

[1] E.E. Fullerton, C.H. Sowers, J.P. Pearson, S.D. Bader, D. Lederman, A general approach to the epitaxial growth of rare-earth-transition-metal films, Appl. Phys. Lett. 69 (1996) 2338–2440.
[2] E.E. Fullerton, J.S. Jiang, C. Rehm, C.H. Sowers, S.D. Bader, J.B. Patel, X.Z. Wu, High coercivity epitaxial Sm–Co films with uniaxial in-plane anisotropy, Appl. Phys. Lett. 71 (1997) 1579–1581.
[3] N. Li, S. Li, E. Zhang, L. Wang, Magnetic property and microstructure of SmCo magnetic recording films, J. Rare Earths 27 (2009) 839–842.
[4] G.T. Landi, A.D. Santos, High-density gas aggregation nanoparticle gun applied to the production of SmCo clusters, J. Mater. Sci. 45 (2010) 4906–4911.
[5] M. Négrier, J. Tuallon, V. Dupuis, C. Tonon, A. Perez, Magnetic properties of Co–Sm mixed-clusters assembled materials, Nanostruct. Mater. 12 (1999) 303–306.
[6] F.J. Cadieu, R. Rani, T. Theodoropoulos, L. Chen, Fully in plane aligned SmCo based films prepared by pulsed laser deposition, J. Appl. Phys. 85 (1999) 5895–5897.
[7] V. Neu, J. Thomas, S. Fähler, B. Holzapfel, L. Schultz, Hard magnetic SmCo thin films prepared by pulsed laser deposition, J. Magn. Magn. Mater. 242–245 (2002) 1290–1293.
[8] A. Singh, V. Neu, R. Tamm, K.S. Rao, S. Fähler, W. Skrotzki, L. Schultz, B. Holzapfel, Growth of epitaxial $SmCo_5$ films on Cr/MgO(1 0 0), Appl. Phys. Lett. 87 (2005) 072505–72513.
[9] A. Singh, R. Tamm, V. Neu, S. Fähler, C.G. Oertel, W. Skrotzki, L. Schultz, B. Holzapfel, Epitaxial growth of highly coercive Sm–Co thin films using pulsed laser deposition, J. Appl. Phys. 97 (2005) 093902–93905.
[10] F. Pigazo, F.J. Palomares, F. Cebollada, J.M. González, Preparation of hard magnetic materials in thin film form, J. Magn. Magn. Mater. 320 (2008) 1966–1971.
[11] L. Alloca, C. Bonavolontà, A. Giardini, T. Lopizzo, A. Morone, M. Valentino, M.F. Verrastro, V. Viggiano, Laser deposition of SmCo thin film and coating on different substrates, Phys. Scr. 78 (2008) 058114–58116.
[12] K. Ono, Y. Kakefuda, R. Okuda, Y. Ishii, S. Kamimura, A. Kitamura, S. Oshima, Organometallic synthesis and magnetic properties of ferromagnetic Sm–Co nanoclusters, J. Appl. Phys. 91 (2002) 8480–8482.
[13] H. Gu, B. Xu, J. Rao, R.K. Zheng, K.K. Fung, C.Y.C. Wong, Chemical synthesis of narrowly dispersed SmCo5 nanoparticles, J. Appl. Phys. 93 (2003) 7589–7591.
[14] Y. Li, X.L. Zhang, R. Qiu, Y.S. Kang, Synthesis and investigation of SmCo5 magnetic particles, Coll. Surf. A Physicochem. Eng. Aspects 313–314 (2008) 621–624.
[15] C.N. Chinnasamy, J.Y. Huang, L.H. Lewis, B. Latha, C. Vittoria, V.G. Harris, Direct chemical synthesis of high coercivity air-stable SmCo nanoblades, Appl. Phys. Lett. 93 (2008) 032505.
[16] N. Toshima, Capped bimetallic and trimetallic nanoparticles for catalysis and information technology, Macromol. Symp. 270 (2008) 27–39.
[17] H.G. Cha, C.W. Kim, E.S. Ji, D.I. Kang, Y.S. Kang, Magnetic property of Sm–Co nanoparticles prepared by solution phase metal salt reduction, J. Nanosci. Nanotechnol. 9 (2009) 7071–7075.

[18] T. Matsushita, T. Iwamoto, M. Inokuchi, N. Toshima, Novel ferromagnetic materials of $SmCo_5$ nanoparticles in single-nanometer size: chemical syntheses and characterization, Nanotechnology 21 (2010) 095603–95609.
[19] E.M. Kirkpatrick, S.A. Majetich, M.E. McHenry, Magnetic properties of single domain samarium cobalt nanoparticles, IEEE Trans. Magn. 32 (1996) 4502–4504.
[20] K.M. Chowdary, A.K. Giri, K. Pellerin, S.A. Majetich, Annealing effects on the coercivity of $SmCo_5$ nanoparticles, J. Appl. Phys. 85 (1999) 4531–4533.
[21] V.M. Chakka, B. Altuncevahir, Z.Q. Jin, Y. Li, J.P. Liu, Magnetic nanoparticles produced by surfactant-assisted ball milling, J. Appl. Phys. 99 (2006), 08E912-3.
[22] Y. Wang, Y. Li, C. Rong, J.P. Liu, Sm–Co hard magnetic nanoparticles prepared by surfactant-assisted ball milling, Nanotechnology 18 (2007) 465701–465704.
[23] N. Poudyal, C. Rong, J.P. Liu, Effects of particle size and composition on coercivity of Sm–Co nanoparticles prepared by surfactant-assisted ball milling, J. Appl. Phys. 107 (2010), 09A703-3.
[24] J. Jakobi, S. Petersen, A. Menéndez-Manjón, P. Wagner, S. Barcikowski, Magnetic alloy nanoparticles from laser ablation in cyclopentanone and their embedding into a photoresist, Langmuir 26 (2010) 6892–6897.
[25] S. Stoyanov, V. Skumryev, Y. Zhang, Y. Huang, G. Hadjipanayis, J. Nogués, High anisotropy Sm–Co nanoparticles: preparation by cluster gun technique and their magnetic properties, J. Appl. Phys. 93 (2003) 7592–7594.
[26] M. Santos, L. Díaz, J.J. Camacho, M. Urbanová, D. Pokorná, J. Šubrt, S. Bakardjieva, Z. Bastl, J. Pola, IR laser-induced metal ablation and dielectric breakdown in benzene, Infrared Phys. Technol. 53 (2010) 23–28.
[27] J. Pola, M. Urbanová, D. Pokorná, J. Šubrt, S. Bakardjieva, P. Bezdička, Z. Bastl, IR laser-induced formation of amorphous Co–C films with crystalline Co, Co_2C and Co_3C nanograins in a graphitic shell, J. Photochem. Photobiol. A Chem. 210 (2010) 153–161.
[28] M. Urbanová, D. Pokorná, S. Bakardjieva, J. Šubrt, Z. Bastl, P. Bezdička, J. Pola, IR laser-induced ablation of Ag in dielectric breakdown of gaseous hydrocarbons: simultaneous occurrence of metastable hcp and stable fcc Ag nanostructures in C:H shell, J. Photochem. Photobiol. A Chem. 213 (2010) 114–122.
[29] D. Pokorná, M. Urbanová, S. Bakardjieva, J. Subrt, J. Pola, Laser ablation of Ga in dielectric breakdown of gaseous hydrocarbons: deposition of ambient-pressure unstable Ga nanophases in carbonaceous environment, J. Photochem. Photobiol. A Chem. 215 (2010) 164–171.
[30] Release 52, International Centre for Diffraction Data, Newton Square, PA, USA, 2002.
[31] J.L. Lábár, M. Adamik, New possibilities in manipulating electron diffraction ring patterns, Microscopy and Microanalysis 7 (Suppl. 2) (2001) 372–373.
[32] J.H. Kiefer, L.J. Mizerka, M.R. Patel, H.-C. Wei, A shock tube investigation of major pathways in the high temperature pyrolysis of benzene, J. Phys. Chem. 89 (1985) 2013–2019.
[33] S. Hüfner, Photoelectron Spectroscopy, 2nd ed., Springer-Verlag, Berlin, 1996, p. 458.
[34] Y. Uwamino, T. Ishizuka, H. Yamatera, X-ray photoelectron spectroscopy of rare-earth compounds, J. Electron Spectrosc. Relat. Phenom. 34 (1984) 67–78.
[35] S. Prawer, K.W. Nugent, Y. Lifshitz, G.D. Lempert, E. Grossman, J. Kulik, I. Avigal, R. Kalish, Systematic variation of the Raman spectra of DLC films as a function of sp^2:sp^3 composition, Diamond Relat. Mater. 5 (1996) 433–438.
[36] J.C. Lascovich, R. Giorgi, S.S. Scaglione, Evaluation of the sp^2/sp^3 ratio in amorphous carbon structure by XPS and XAES, Appl. Surf. Sci. 47 (1991) 17–21.
[37] A.A. Galuska, H.H. Madden, R.E. Allred, Electron spectroscopy of graphite oxide and amorphous carbon, Appl. Surf. Sci. 32 (1988) 253–272.
[38] R.G.J. Miller, H.A. Willis (Eds.), Infrared Structural Correlation Tables and Data Cards, Heyden & Son Ltd., Spectrum House, London, 1969.
[39] I. Morjan, I. Voicu, F. Dumitrache, I. Sandu, I. Soare, R. Alexandrescu, E. Vasile, I. Pasuk, R.M.D. Brydson, H. Daniels, B. Rand, Carbon nanopowders from continuous-wave CO_2 laser-induced pyrolysis of ethylene, Carbon 41 (2003) 2913–2921.
[40] N. Herlin, I. Bohn, C. Reynaud, M. Cauchetier, A. Galvez, J.N. Rouzaud, Nanoparticles produced by laser pyrolysis of hydrocarbons: analogy with carbon cosmic dust, Astron. Astrophys. 330 (1998) 1127–1135.
[41] I. Morjan, I. Voicu, R. Alexandrescu, I. Pasuk, I. Sandu, F. Dumitrache, I. Soare, T.C. Fleaca, M. Ploscaeu, V. Ciupina, H. Daniels, A. Westwood, B. Rand, Gas composition in laser pyrolysis of hydrocarbon-based mixtures: influence on soot morphology, Carbon 42 (2004) 1269–1273.
[42] J. Pola, S. Bakardjieva, M. Maryško, V. Vorlíček, J. Šubrt, Z. Bastl, A. Galíková, A. Ouchi, Laser-induced conversion of silica into nano-sized carbon–polyoxocarbosilane composites, J. Phys. Chem. C 111 (2007) 16818–16826.
[43] J. Pola, A. Ouchi, M. Maryško, V. Vorlíček, J. Šubrt, S. Bakardjieva, Z. Bastl, UV laser nanomagnetic soot from gaseous benzene–acetonitrile mixture, J. Photochem. Photobiol. A 220 (2011) 188–194.